Experimental Thermal and Fluid Science 42 (2012) 219–229

Contents lists available at SciVerse ScienceDirect

Experimental Thermal and Fluid Science

journal homepage: www.elsevier.com/locate/etfs

Infra-red thermography of laminar heat transfer during early thermal development inside a square mini-channel

Balkrishna Mehta, Sameer Khandekar *

Department of Mechanical Engineering, Indian Institute of Technology Kanpur, Kanpur (UP) 208016, India

ARTICLE INFO

Article history:
Received 16 December 2011
Received in revised form 29 April 2012
Accepted 13 May 2012
Available online 7 June 2012

Keywords:
Mini-channel
Thermally developing flow
Infra-red thermography
Conjugate heat transfer
Non-intrusive technique
Experiments and numerical modeling

ABSTRACT

Infra-red thermography (IRT) has been employed to experimentally scrutinize the thermo-hydrodynamics of very early part of hydrodynamically fully developed, but thermally developing, internal laminar flow of water ($850 \geqslant Re \geqslant 100$) in a mini-channel of square cross-section (5 mm × 5 mm; aspect ratio = 1.0; D_{hyd} 5 mm). The channel is machined on that face of an aluminum substrate whose dimensions are 11 mm × 140 mm; the total width of the substrate being 45 mm. A constant heat flux boundary condition is provided on the substrate face which is opposite to that on which the mini-channel is machined. Thus, the mini-channel receives heat from three sides; the fourth side being covered by an insulating poly-carbonate material. IRT provides non-intrusive and high-resolution spatial measurement of local wall temperature in the streamwise direction. By assuming a one-dimensional heat transfer model in the transverse direction, the local value of heat flux and therefore the Nusselt number, in the thermally developing region, can be estimated. Moreover, a 3D conjugate heat transfer numerical model, exactly corresponding to the real experimental conditions, has also been developed. The conjugate effects in the experiment arising due to the substrate, as well as the high heat transfer coefficient in the early thermal development zone, are analyzed. The errors and discrepancy in the *in situ* boundary conditions which may creep in due to such effects, especially in the estimation of transport coefficients in the developing flow region, are scrutinized and delineated. It is concluded that experimental estimation of local heat flux is a primary requirement for minimizing the errors in estimating local Nusselt number in developing flows. This in turn, necessitates the use of non-intrusive field measurement techniques, such as IRT.

1. Introduction

In recent years, there is a rapid growth of applications which require high heat flux removal from confined geometries. To meet this requirement, miniaturization of species transport devices, which leads to high surface to volume ratio, is required. However, miniaturization of the thermo-fluidic systems has some inherent disadvantages. For example, in small geometries, generation of turbulence is not feasible and cannot be generally used as a means for heat transfer enhancement. Transport enhancement techniques in the laminar region thus need to be understood and implemented. Hydrodynamically and/or thermally developing flows are inherently suited for passively achieving high transport coefficients. Common examples of such flows occur in electronics thermal management, cooling of laser devices, space thermal management, MEMS devices for biological and chemical reactors, micro-scale chemical reactors and heat exchangers, etc.

Laminar flows, for a range of specified boundary conditions, are quite well understood in the macroscopic domain, both experimentally and analytically [1]. Extrapolating these ideas to micro or mini scales poses several challenges, such as: (a) the ratio of area of cross sections for the heat flow in the solid substrate encompassing the flow channels to that of the fluid flow domain (A_{sf}) is usually either comparable or can even be quite large. Due to this, the ensuing conjugate nature of heat transfer cannot be ignored. The heat transfer boundary condition which the fluid actually experiences at the solid fluid boundary significantly deviates from the conventional UHF (Uniform Heat Flux) or UWT (Uniform Wall Temperature), as mathematically or experimentally conceived [2–4], (b) intrusive point measurements for determining flow characteristics and transport coefficients, for example conventional thermometry and velocimetry, also defeat the purpose as they disrupt the thermal and hydrodynamic flow behavior, (c) localized 3-dimensional effects get manifested more profoundly in these small scale systems leading to erroneous estimation of transport parameters, and, (d) developing flows, especially immediately after entrance, provide very high heat transfer and therefore require higher resolution of temperature measurement for heat transfer estimation. These limitations necessitate that the metrology of such systems be, as far as possible, non-intrusive and preferably should provide

* Corresponding author. Tel.: +91 512 259 7038; fax: +91 512 259 7408.
E-mail address: samkhan@iitk.ac.in (S. Khandekar).

0894-1777/$ - see front matter © 2012 Elsevier Inc. All rights reserved.
http://dx.doi.org/10.1016/j.expthermflusci.2012.05.007

Nomenclature

A	area (m^2)
c_p	specific heat at constant pressure (J/kg K)
D	diameter (m)
h	heat transfer coefficient (W/m^2 K)
k	thermal conductivity (W/m K)
L	length (m)
M	axial heat conduction number (–)
m	fin parameter $\sqrt{p \cdot h_{amb}/(k_{fin} \cdot A_{fin})}$ (1/m)
p	perimeter (m)
Q	Heat power (W)
q''	heat flux (W/m^2)
T	temperature (K)
T^*	non-dimensional temperature (–)
u	velocity (m/s)
Z	distance from inlet (m)
Z_h	hydrodynamic non-dimensional distance ($=Z/\mathrm{Re}\cdot D_h$)
Z^*	thermal non-dimensional distance ($=Z/\mathrm{Re}\cdot\mathrm{Pr}\cdot D_h$)

Greek symbols

δ	thickness (m)
μ	dynamic viscosity (Pa s)
ρ	mass density (kg/m^3)
φ	heat flux ratio ($= q''_z/q''$) (–)

Non-dimensional numbers

Bi	Biot number ($h\cdot\delta/k_s$)
Nu	Nusselt number ($h\cdot D_h/k_f$)
Pr	Prandtl number ($\mu_f\cdot c_p/k_f$)
Re	Reynolds number ($\rho_f\cdot u\cdot D_h/\mu_f$)

Subscripts

amb	ambient
b	base
c	characteristics
f	fluid
fd	fully developed
fin	related to a fin
h	hydraulic, hydrodynamic
hp	heated perimeter
i	inlet
m	mean
o	outlet
sf	solid–fluid
t	thermal
w	wall
z	local value

multi-dimensional high-resolution spatio-temporal information of the process parameters.

IRT is a rapidly developing technique for spatio-temporal thermal measurements for research purposes. As compared to other non-intrusive techniques like Liquid Crystal Thermography (LCT), it is much more versatile, repeatable and relatively easier to implement. Various issues which need to be addressed for quantitative estimation of process parameters from the measured IR energy spectrum include, amongst others, (i) calibration of the sensor (ii) determination of the correct emissivity of the radiating surface (iii) transmissivity of the participating media and IR optics (iv) isolation of noise during digitalization [5].

Klassen et al. [6] used IRT to obtain the transient surface temperature distribution in the neighborhood of an evaporating droplet. Hetsroni et al. [7] employed a hot foil IRT technique for the measurement of heat transfer in single-phase as well as two-phase flows. Use of IRT in applications involving convective flows e.g., jet impingements on rotating disks, jet in cross flow and internal flows etc., has been reported by Astarita et al. [8]. Exploiting the capability of IRT at small scales, Hetsroni et al. [9] have performed field measurements of surface temperature of a heated capillary tube. This method was based on the measurement of local temperatures on the air-side surface of a thin heater, whereas the other side of the heater was subjected to a liquid flow; the heat transfer coefficient between the wall and inner flow was determined. Montelpare and Ricci [10] investigated the convective heat transfer coefficient of liquid cooled short pin fins using IRT. In this study, lateral surface temperature was estimated from the top surface temperature distribution captured by IR camera. Kakuta et al. [11] used IRT for measuring the temperature of sub-millimeter-thick water; the temperature distribution due to diffusion in the water was measured and results were compared with the numerical simulation by using the conduction model. In another study, Buchlin [12] used IRT for the quantitative estimation of convective heat transfer of high enthalpy flows, multi-jet systems and systems with turbulators ribs. The author also highlights the critical data reduction parameters for correct temperature estimation from IR radiation data. Recently, Hetsroni et al. [13] have implemented IRT on micro-channel and micro-fluidic systems and have highlighted the major problems encountered in the process. Brutin et al. [14] investigated the thermal motion inside the sessile drop kept at the heated surface by using IRT. Transient measurements of evaporation process were done to experimentally capture the different phases involved in it. Hemadri et al. [15] have employed IRT for the measurement of spatio-temporal 2D temperature fields on a radiator plate embedded with a pulsating heat pipe. In this study, quasi-steady state spatial surface isotherms on the radiator plate were successfully captured and the results were in good agreement to those predicted by their numerical simulations.

In the recent past, the frequency of reports describing the utilization of IRT for studying convective flows is rapidly increasing. State-of-the-art camera systems available today can provide sufficient spatio-temporal information to elucidate quantitative conclusions regarding mini and micro-scale convective flow situations, provided of course, due diligence is exercised on sources of error generation in such systems [16].

In the present study, the primary aim is to experimentally determine the local laminar heat transfer coefficient along the streamwise direction in single-phase internal convective flows. The study focuses on the very early part of thermal boundary layer development wherein the transport coefficients, as well as their axial gradients along the streamwise direction, are very high and the measurement is challenging. As noted earlier, most practical systems having mini/micro dimensions will be subjected to conjugate effects. In recent years, many studies report the quantitative estimation of the effect of conjugate heat transfer on convective flows in mini/micro scale geometries on the convective transport. Lee et al. [17] and Lee and Garimella [18] conducted a 3-D conjugate laminar heat transfer analysis, including entrance effects, for single channels as well as micro-channel heat sinks, subjected to uniform heat flux imposed on the bottom of the substrate. Operating regimes and boundary conditions wherein conjugate effects become important were identified. Based on numerical simulations they have proposed correlations to predict local and average

Nusselt number under such conditions. Celata et al. [19] observed the behavior of single-phase forced convective heat transfer in micro-tubes and have discussed the difficulties encountered during measurements, especially the flow entrance effects and the conjugate nature of heat transfer. An overall decrease in Nu, for all flow Re up to transition to turbulence, is the most important conclusion, attributed to conjugate nature of heat transfer. Liu et al. [20] experimentally studied the axial heat conduction in thick walled micro-tube using IR thermography and proposed a correlation between axial heat conduction and convective heat transfer, based on experimental results. Nonino et al. [21] analyzed the effect of axial heat conduction for simultaneously developing laminar flow in the circular micro-channel with the aim of pointing out the influence of geometrical parameters and the solid–fluid conductivity ratio (k_{sf}) on the heat transfer coefficient.

If accurate heat transfer coefficient needs to be experimentally determined in a given system, it is imperative to judge the extent of axial back conduction and other conjugate/multi-dimensional effects which may distort the correctness of the estimation of transfer coefficients, vis-à-vis the mathematically ideal boundary conditions; most analytical solutions are usually applicable for the latter case. Thus, the importance of local heat flux carried by the fluid along the flow direction cannot be underestimated. Non-intrusive, reliable techniques having the capability of resolving the information spatio-temporally need to be developed to understand the physics under such boundary conditions; here, an attempt has been made to use IR thermography for metrology under such situations. Baseline measurements are bench-marked against available analytical solutions. In addition, CFD simulations are also carried out on a commercial platform for parametric studies which gives important insight into further development of experimental technique to study internal convective flows using IRT.

2. Experimental details and procedure

The primary idea of the experimental design is to create an extended surface fin structure, one end of which is subjected to a constant heat flux boundary condition and the other end is subjected to a convective heat transfer boundary condition. As the heater is located away from the channel, the thermal boundary condition at the fluid-wall interface is not identified as the conventional Uniform Heat Flux (UHF) or Uniform Wall Temperature (UWT). Such a configuration, which is frequently encountered in real-time applications, makes the problem inherently conjugate in nature. The goal is to reduce the effect of axial conduction through the solid fin substrate in the streamwise direction and simultaneously to reduce the effective Biot number in the transverse direction at the channel wall, so as to get a good estimate of the local heat transfer coefficient. To establish this methodology for correct estimation, the conjugate nature of the problems needs to be fully understood and the design of the setup should be such that effects of axial conduction on the estimation of local heat transfer are quantifiable and as far as possible, minimized. The experimental facility, to meet the above requirements, is schematically shown in Fig. 1a.

The test section consisted of single square mini-channel (w = 5.0 mm, δ_f = 5.0 mm; D_h = 5.0 mm, length in the streamwise Z direction = 140 mm), machined on an aluminum substrate (k = 180 W/m K) of 11 mm × 45 mm × 140 mm. The top of the channel was covered by a poly-carbonate sheet (5.0 mm thick, k = 0.22 W/m K), providing necessary insulation from top of the test section, as shown in Fig. 1a. The area (A_{hp}) of the fluid–solid interface, considering only three sides of the aluminum substrate from where heat enters the fluid is equal to 5 mm × 140 mm × 3 = 2100 mm^2. An unheated duct length of 200 mm, having the same flow cross-section, was provided before the entry to the heated test section for achieving hydrodynamic flow development under all flow Reynolds numbers covered in this test, i.e. 850 ⩾ Re ⩾ 100.

For providing constant heat flux boundary condition (q'') at the base of the aluminum substrate, a cylindrical DC supplied cartridge heater (diameter: 15 mm and length: 140 mm) was inserted, with the application of conducting thermal paste (metal oxide filled silicon oil paste supplied by RS components®, k = 2.9 W/m K), as shown; as has been noted earlier, the upper surface of the flow channel was insulated. Digital multi-meters (accuracy ±0.1 V and ±0.01 A) were used to measure the electrical power dissipation of the heater. The base area of the aluminum fin structure through which heat passes for eventual dissipation to the flowing fluid (A_b) is 11 mm × 140 mm = 1540 mm^2. The ratio A_{hp}/A_b equals 1.36 while the ratio of cross sectional area of solid to fluid ($A_{sf} = A_s/A_f$) is 18.8.

The working fluid (distilled, degassed and deionized water) at a fixed temperature, maintained by a constant temperature bath (Make: Julabo® F34 ME, accuracy ±0.1 K), was made to pass through the mini-channel. The fluid temperatures at inlet and outlet of the test section respectively, were measured by suitably located K-type thermocouples (Omega®, 0.5 mm bead diameter, accuracy ±0.1 after calibration). All the surfaces of fin-substrate were completely insulated except an area of 25 mm × 130 mm (see zone ABCD in Fig. 1) at the front surface which was covered by a 5 mm thick Infra-red transmitting CaF_2 glass window (Make: Crystran®; Transmissivity: 95%, for wavelength 2–7 μm; Refractive index = 1.399 at 5 μm; k = 9.71 W m^{-1} K^{-1}), as shown in Fig. 1. This window facilitated the recording of spatial IR thermographic profiles of the front surface of the fin-substrate. For bench-marking the camera, and to measure the channel wall temperature at the back surface (behind the surface on which IR transparent glass was fitted; see Fig. 1a), four more K-type pre-calibrated (against Pt-100 NIST traceable calibration) thermocouples $T_{z\text{-}1}$ to $T_{z\text{-}4}$ were attached in the flow direction along the channel length at 10 mm, 50 mm, 90 mm and 130 mm, respectively from the heated test section inlet, as shown in Fig. 1. Thermocouple data acquisition was carried out at 1 Hz by using a high precision 12 bit PCI-DAQ card (Make: National Instruments®, PCI-6024E/TBX-68 connector block). The IR camera used (Make: FLIR, Model: SC4000; Indium Antimonide detector array) had an operational spectral band of 3–5 μm, 14 bit signal digitization and a Noise Equivalent Temperature Difference of less than 0.02 K at 30 °C. IR images were acquired and post processed by using ThermaCAM™ Researcher-V2.9 software [16].

Heat losses to the environment from the setup were estimated based on the conservation of energy – the difference between the electrical energy supplied to the channel and that received by the working fluid after steady state operation was achieved; this was found to be always less than ~7–13%, depending on the heat input. The Prandtl number of the fluid, as reported here, is based on the fluid inlet temperature.

3. Modeling and numerical simulation

The governing equations for the conjugate convective flow problem are as follows:

Continuity equation:

$$\nabla \cdot \vec{u} = 0 \tag{1}$$

Momentum equation:

$$\rho(\vec{u} \cdot \nabla \vec{u}) = -\nabla p + \mu \nabla^2 \vec{u} \tag{2}$$

Energy equation:

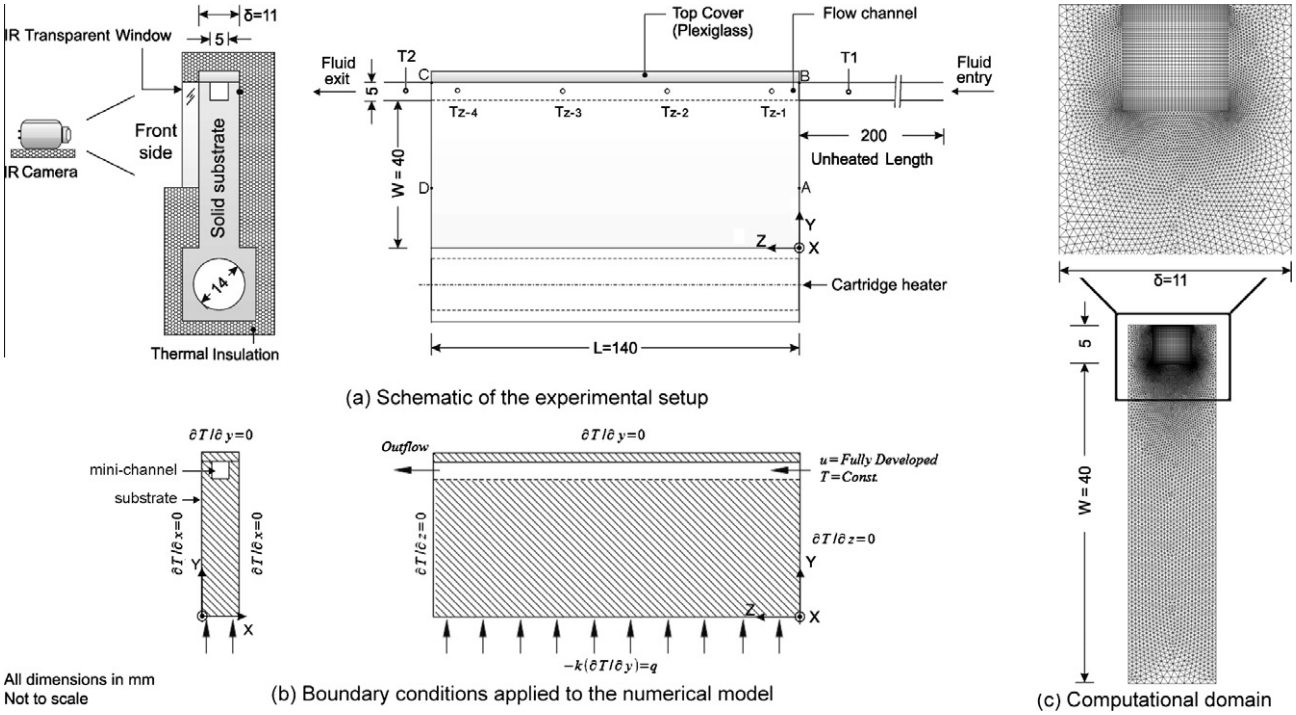

Fig. 1. (a) Schematic of the experimental set-up, (b) mathematical domain description with applied boundary conditions and, (c) a typical computational domain for the solid and the fluid sections.

$$\vec{u}\cdot\nabla T = \alpha\nabla^2 T \tag{3}$$

Boundary conditions:

In fluid domain, fully developed velocity profile at the inlet is given by [22]:

$$u(x,y) = \frac{16}{\pi^2}\sum_{m=0}^{\infty}\sum_{n=0}^{\infty}\frac{(-1)^{m+n}}{(2m+1)(2n+1)}\cos\frac{(2m+1)\pi x}{2a}\cos\frac{(2n+1)\pi y}{2a};\quad T = T_i \tag{4}$$

At the flow outlet, the standard outflow condition has been applied, given by:

$$\frac{\partial\Phi}{\partial z} = 0;\quad \text{where } \Phi = u, v, w, T \tag{5}$$

In the solid domain,

$$\text{at } z = 0 \text{ and } L: \frac{\partial T}{\partial z} = 0 \tag{6}$$

$$\text{at } x = 0 \text{ and } \delta: \frac{\partial T}{\partial x} = 0 \tag{7}$$

$$\text{at } y = 0: -k\frac{\partial T}{\partial y} = q'';\quad y = W: \frac{\partial T}{\partial y} = 0 \tag{8}$$

To solve the above set of equations, numerical simulations have been carried out using commercial software, Ansys-Fluent®6.3.26. A 3D model representing the exact dimensions of the experimental setup was constructed using the grid generator GAMBIT-V-2.3®, as detailed in Fig. 1b and c. Before freezing the computational grid size, a grid independence test was carried out. As an example, local Nusselt number obtained for the present problem for three different grids of 20 × 20 × 100, 25 × 25 × 140 and 35 × 35 × 200, for Re = 100, is shown in Fig. 2. Benchmark results from developing as well as fully developed flow, [1] with constant heat flux applied at the fluid–solid interface were also verified before taking up the conjugate problem, as shown. The local Nusselt number, at the

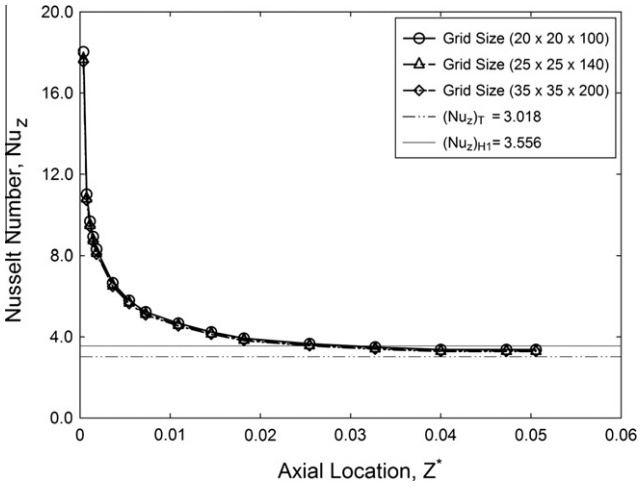

Fig. 2. Grid independence test for present conjugate domain.

fully developed flow regime, changed by 1.06% from the grid-size of 20 × 20 × 100 to 25 × 25 × 140, and changed by less than 1%, upon further refinement to grid-size of 35 × 35 × 200. As no appreciable change was observed by using the above three sets of grids, the intermediate grid size of 25 × 25 × 140 for the fluid domain and 25 × 90 × 140 for solid domain, in the *X*, *Y* and *Z* direction respectively, was chosen. Finer meshes were used near to the solid–fluid interface to resolve the local gradients accurately with successive ratio of 1.03 (smallest cell size in the actual physical domain representing the fluid was 10^{-5} m which provided approximately five grid points within the viscous length scale). 'Green-Gauss cell based' theorem is used to compute the scalars at the cell centers. Face values of the scalars are calculated by weighted arithmetic averaging of the neighboring values at cell centers. 'SIMPLE' algorithm was employed for the pressure–velocity coupling. For descretization of momentum and energy equation, 'second order

upwind' scheme has been applied. Interpolation of pressure is done by the 'Standard' scheme. For applying the fully developed inlet velocity profile condition, defined by Eq. (4) [22], a user defined function was written. Absolute convergence criterion set for momentum was 10^{-6} and for that for energy was 10^{-8}.

4. Benchmarking of IR thermography

Prior to using the IR camera for estimation of local heat transfer coefficients, its own bench marking exercise was performed to instill confidence in the subsequent estimation of local heat transfer coefficient in the thermally developing flow. This benchmarking test is described below.

Cole et al. [23] have analytically solved the diffusion equation in an extended surface fin of constant cross sectional area subjected to constant heat flux q'' at the fin base. Three different boundary conditions at the fin tip were considered, i.e. insulated tip, convective tip, and tip at the ambient temperature (infinitely long fin). The steady state analytical solution is obtained for the insulated tip boundary condition by reducing the equation for infinite time. The reduced equation is given as [23]:

$$\frac{T(y)-T_{amb}}{(q''_{fin}\cdot L_{fin}/k_{fin})}=\frac{(e^{-m(2L_{fin}-y)}+e^{-m\cdot y})}{m\cdot L_{fin}(1-e^{-2m\cdot L_{fin}})} \tag{9}$$

To independently verify the IR camera measurements, an experimental setup was made to compare the temperature profiles, as described analytically by Eq. (9). A simple aluminum plate 185 mm × 85 mm × 15 mm was subjected to the same boundary condition as considered by Cole et al. [23], i.e., one face (85 mm × 15 mm) of the plate was subjected to constant heat flux and corresponding opposite face was insulated, whereas all other faces were exposed and subjected to natural convective boundary conditions, as shown in Fig. 3a. The spatial IR thermograph obtained after coating the exposed surfaces of the aluminum plate with carbon-black (emissivity, $\varepsilon \geqslant 0.96$) is shown in Fig. 3b. The non-dimensional surface temperature profile obtained on Regions of Interest (ROI) 1–4, as detailed in Fig. 3b, are shown in Fig. 3c. Also shown in the Fig. 3c are the temperatures obtained by the six thermocouples $T_{y\text{-}1}$ to $T_{y\text{-}6}$, which closely match the IR data. The fact that the Biot number based on thickness in the x-direction ($h\cdot\delta/k_s = 0.00067$), is very small, temperature gradients are expected to be only in the y-direction, as is also confirmed by the IR and thermocouple data; the system emulates an extended surface one-dimensional fin highlighted by the fact that the temperatures of all ROIs (1 though 4), taken at different axial locations (z-direction) are indeed overlapping.

The only unknown in Eq. (9) is the outside ambient natural convective heat transfer coefficient. As seen from Fig. 3c, the obtained temperature profiles from experiment correspond to a heat transfer coefficients in the range of 8–9 W/m^2 K, as per Eq. (9). This value of natural convective heat transfer clearly suggests that radiation heat transfer is playing a sizable role in the total heat transfer. To verify this, the same experiment was conducted with an uncoated aluminum surface with natural finish ($\varepsilon \sim 0.21$, [16]), without any carbon-black coating. Of course, in such a situation when the surface emissivity is low, IR camera cannot be expected to give reasonable results. However, the measured thermocouple data $T_{y\text{-}1}$ to $T_{y\text{-}6}$ corresponding to such low emissivity of the exposed aluminum surface is also shown in Fig. 3c. For this case, the estimated heat transfer coefficient comes out to be between 4.5 W/m^2 K and 5 W/m^2 K, which is indeed a very good estimate of natural convective coefficient under such conditions, [24]. The fact that radiation plays a significant role under natural convective conditions, even at lower operating temperatures, is clearly highlighted by many studies, including, for example, by Audunsun and Gebhart [25].

5. Data reduction

The peripheral average local Nusselt number (Nu_z) for the square duct employed in the present study is defined as:

$$Nu_z = h_z \cdot D_h/k_f \tag{10}$$

where the local heat transfer coefficient is defined as follows:

$$h_z = q''_z/(T_{wm}-T_{fm}), \text{and,} \tag{11}$$

$$q''_z = -k_s(\partial T/\partial y)_z \tag{12}$$

The heat flux ratio ϕ is defined as the ratio of the local heat flux q''_z (based on A_{hp}) to that of the applied constant heat flux at the bottom of the substrate q'' (based on A_b), i.e.,

$$\phi = \frac{q''_z}{q''} \tag{13}$$

For all subsequent data processing, unless otherwise stated, the following two definitions for the wall and fluid temperatures were used respectively.

5.1. For experimental data reduction

T_{wm} is the local mean temperature of front surface of the channel wall, as measured by IR camera and T_{fm} is the linearly interpolated value between the fluid inlet and outlet temperatures at channel cross-section corresponding to the two thermocouples locations T_{in} and T_{out} (Fig. 1a).

Although, in the case of experiments, thermocouples could have been inserted in the flow to measure the fluid temperature, it was observed that by doing so, the velocity boundary layer was getting disturbed and the assumption of hydrodynamically fully developed flow was getting compromised. In fact, during such trials, the local Nusselt number was coming to be higher than the predictions for hydrodynamically fully developed but thermally developing flows. Therefore, to capture the Nusselt number as close as possible, explicitly in the thermal development region only, decision was made not to disturb the flow by inserting thermocouples in the channels. As will be seen later, although this makes the measurements non-intrusive, capturing the non-linear increase of fluid temperature in the channel, under the situations when axial back-conduction dominates, is then not recordable. Thus, the assumption of a linear temperature rise of the fluid as it passes through the channel is only valid so far as the conjugate effects are negligible. These aspects and the limitations thereof will be discussed subsequently. Local heat flux along the channel, q''_z in Eq. (12), is calculated from the IR thermograms; the local gradient of temperature and the k_s being known, assuming essentially 1D-conduction at the interface as described in Fig. 4, provides the necessary estimation of local heat flux q''_z.

5.2. For numerical data reduction

T_{wm} is the peripheral averaged wall temperature at location of interest along the channel; T_{fm} is the area averaged fluid temperature at the fluid cross-section of interest along the channel and q''_z is the local heat flux at the fluid–solid interface, as numerically obtained from the local gradient.

In the case of simulations, the local fluid temperature is explicitly known; this was not the case with the experiments, as discussed earlier.

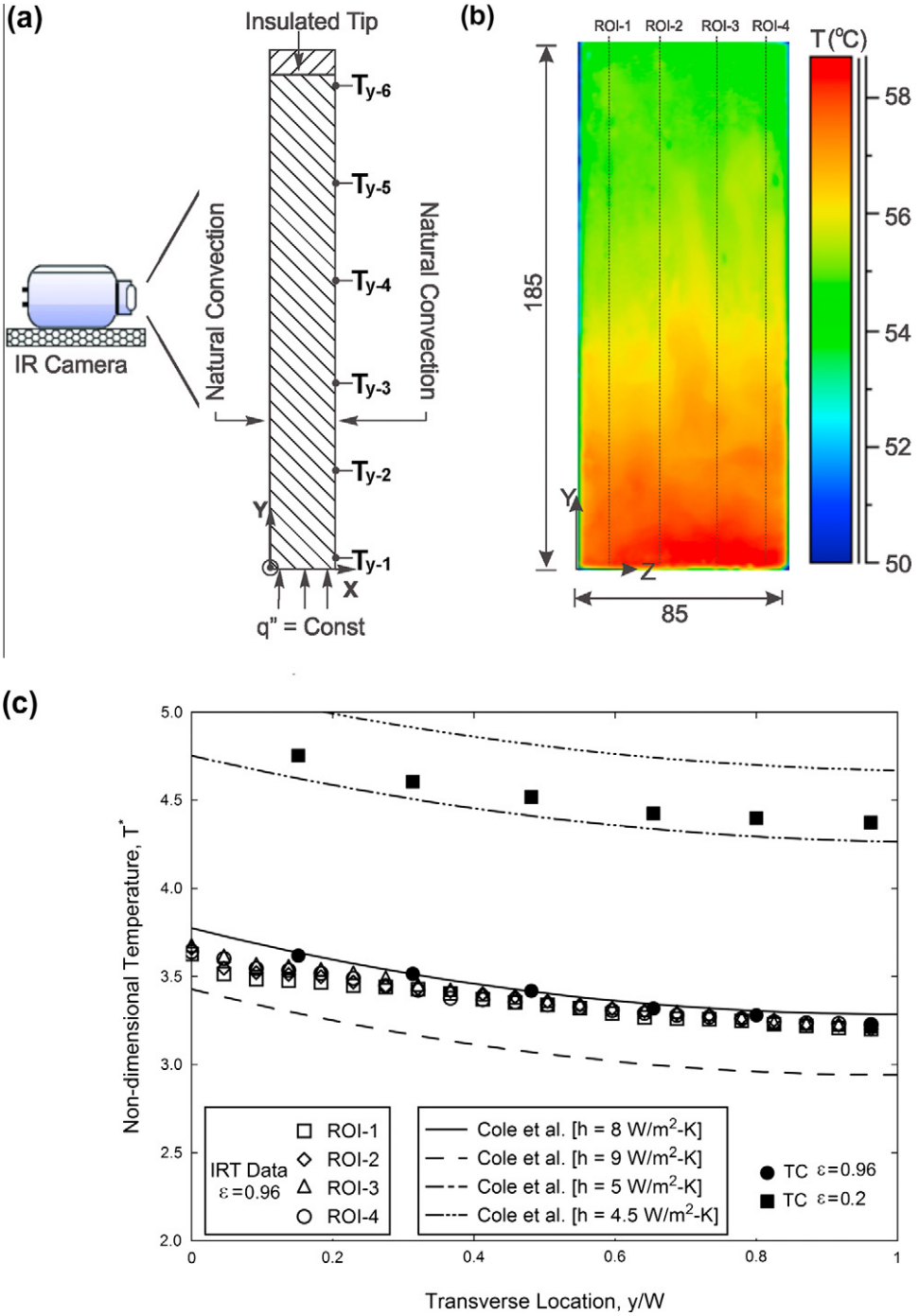

Fig. 3. (a) Schematic of fin experimental set-up. (b) IR thermogram with different regions of interest (ROIs). (c) Comparison of experimental temperature profile with analytical solution for different emissivity.

6. Results and discussion

The calibration of the IR camera on the experimental setup, as detailed in Section 2, is reported here, prior to the discussion on the detailed results of the experiments. It is imperative to perform this calibration exercise, *in situ*, so as to benchmark the emissivity correction factor of the carbon-black coating against standard pre-calibrated thermocouples installed on the experimental setup. This exercise is vital, over and above the benchmarking of the camera measurements against standard boundary conditions, as detailed in Section 5. The *in situ* comparison of axial wall temperature measurements obtained by the four thermocouples $T_{z\text{-}1}$ to $T_{z\text{-}4}$ and the IR thermography at flow Reynolds number 100, 330, 550, and 850 are shown in Fig. 5. The thermocouples are placed at the back surface of the channel wall, while temperature of front surface which is coated by carbon-black, is captured by IR camera. As noted earlier, the Biot number in the *X*-direction is extremely small, there is no temperature gradient expected in this direction. As can be seen, the comparison is excellent for an emissivity value of the carbon-black taken to be 0.964.

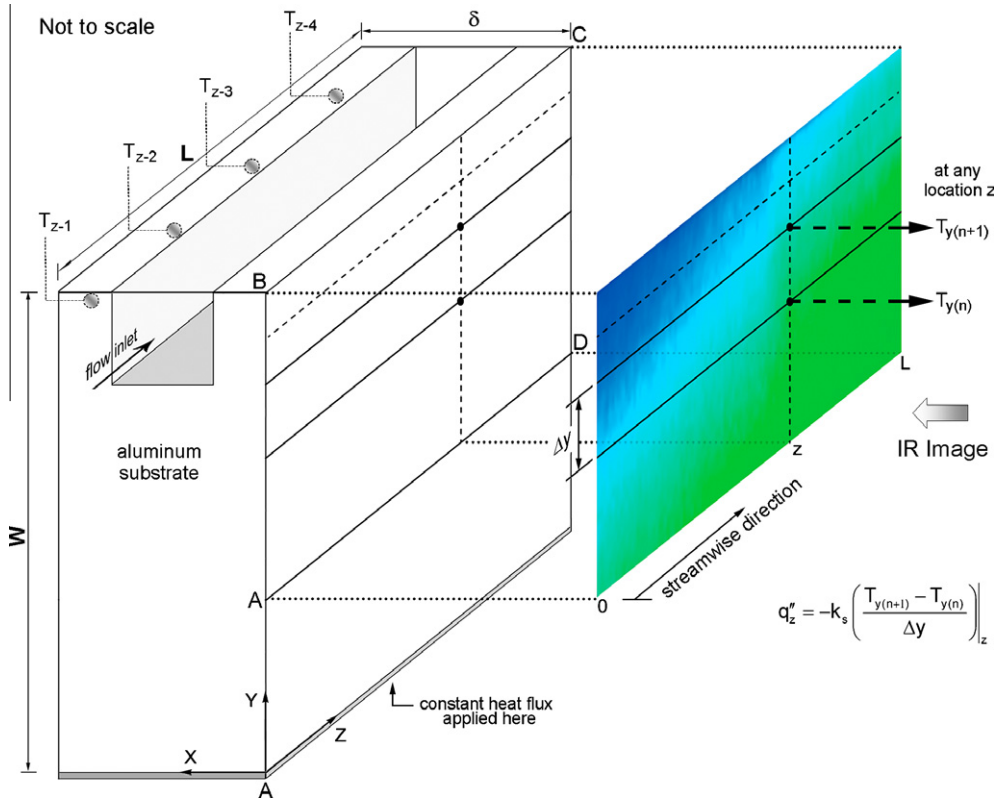

Fig. 4. Experimental data reduction from the IR thermogram.

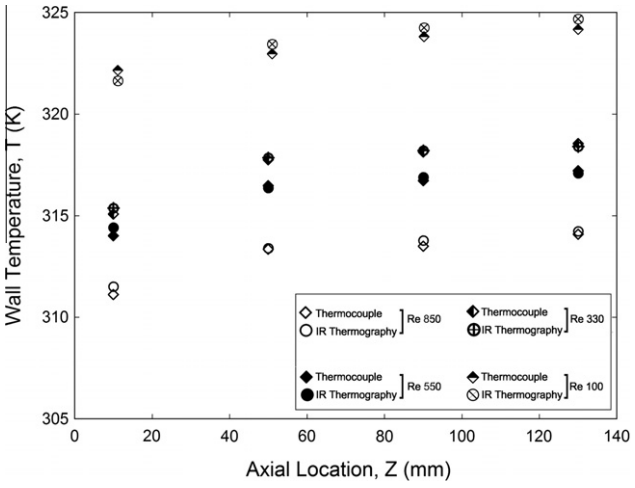

Fig. 5. In-situ calibration of IR camera with thermocouples.

Fig. 6a–d shows the axial variation of local Nusselt number, Nu_z along the streamwise direction in the channel, for flow Reynolds numbers 100, 330, 550 and 850, respectively. For each sub-figure, the IR thermograph of the front surface ABCD of the substrate (refer Fig. 4) is also shown in the inset, with the appropriate temperature scale. For reference, the fully developed value of Nusselt number at constant heat flux boundary condition at the fluid–solid interface, $(Nu_z)_{H1}$ and at constant temperature boundary condition $(Nu_z)_T$ is depicted in the figure. For further benchmarking, a correlation of $(Nu_z)_{H1}$, proposed for a four side heated square channel having thermally developing flow, and with no conjugate effects, by Lee and Garimella [18], is also shown. It can be noted that, as the flow Re decreases from 850 to 100, the non-dimensional thermal-entry length z^*, corresponding to the maximum length of the channel (i.e. 140 mm), increases. For Re = 850, the channel length represents about one-hundredth ($z^* \sim 0.006$) of the thermal boundary layer development length. For the lowest Re tested, the maximum z^* increase to 0.015. Given the fact that full thermal boundary layer development is expected to occur only after $z^* \sim 0.05$ (for non-circular channels, this may be even higher [26,27]), the streamwise wall temperature variation can be elegantly captured for very early thermal entry lengths. The isotherm contours in the respective figure insets, clearly show that, due to very high heat transfer coefficient achieved in the thermal entry zone, the heat flux cannot remain constant at the fluid–solid interface of the channel duct. This is quite different as compared to the case when a constant heat flux boundary condition is directly applied at the fluid–solid interface, as reported in [17,18]. For this latter case, for achieving high heat transfer coefficients in the thermal entry zone, the corresponding temperature difference between the wall and the fluid must decrease, as the local flux has to remain constant by virtue of the applied boundary condition. For Flow Re = 100, the thermal boundary layer nearly fully develops inside the channel length.

In Fig. 6, the experimental results are also plotted along with the corresponding numerical simulations wherein it can be seen that agreement in results is reasonably good. At certain locations along the channel, experimental data shows some abrupt kinks. This can be attributed to (i) some local variation of emissivity of the carbon-black which may be due to uneven thickness/non-homogeneity of particle diameters of the coating (ii) some inherent non-isotropic nature of the IR transparent glass which was used in the experiment. Experiments were repeated several times and the scatter in the respective measurements was inconsequential.

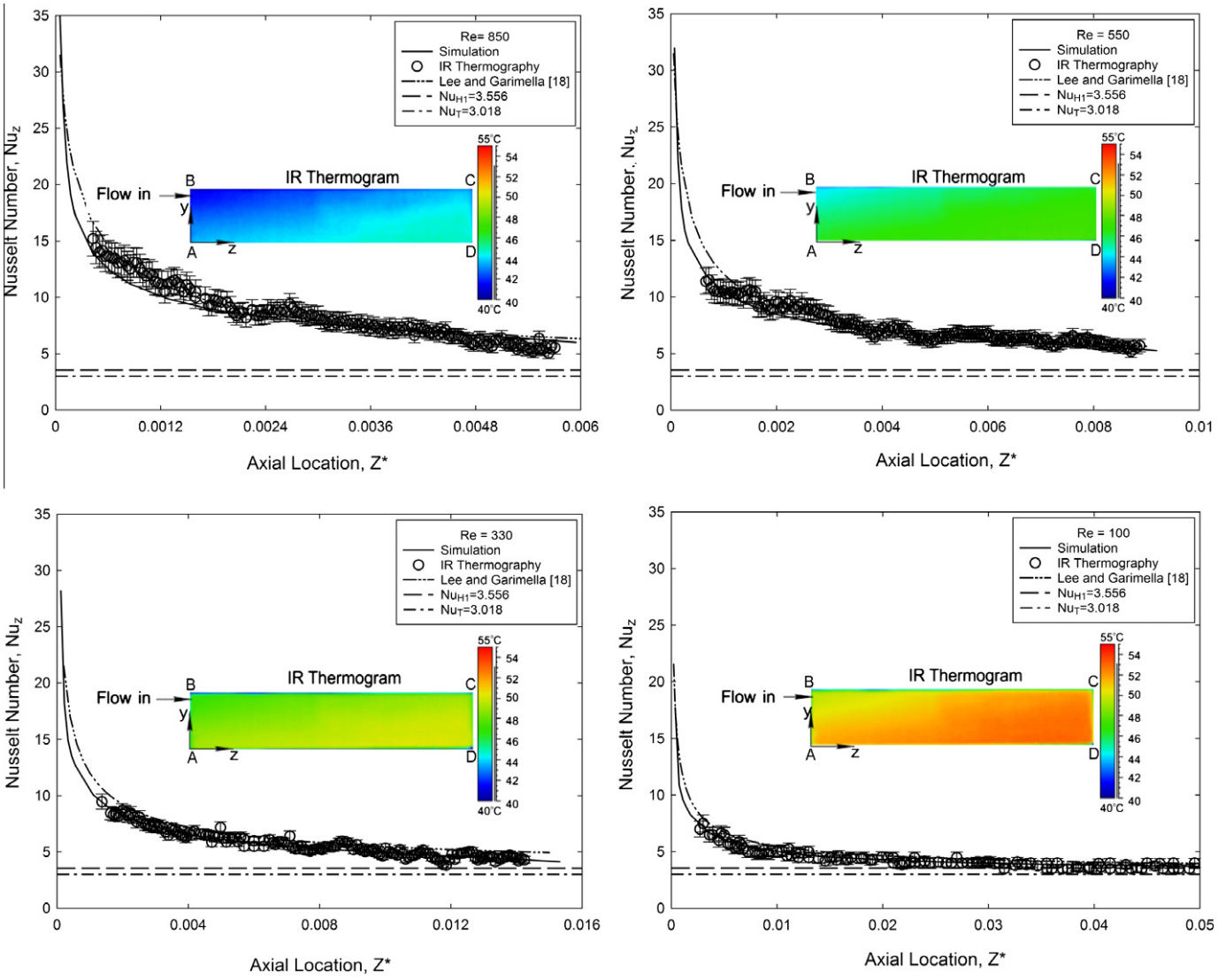

Fig. 6. Comparison of Local Nu_z obtained from simulation and experiments at different flow Re. The inset of each figure shows the thermographic isotherm contours.

Next, as the flow conditions are necessarily conjugate in nature, the issue of axial conduction in the substrate and its effect on the estimation of Nu_z has been scrutinized. As noted earlier in the thermographs of Fig. 6a–d, the fluid–solid interface at the duct periphery does not experience a constant heat flux; the local heat flux indeed varies along the flow direction. The pertinent question is: to what extent this variation affects the estimation of the local Nusselt number Nu_z? Fig. 7 shows the local Nusselt number obtained from the simulation results of for two cases (i) aluminum substrate, as used in the experiments, where $k_{sf} = (k_s/k_f) = 300$ and, (ii) a stainless steel substrate, where $k_{sf} = 26.6$. Corresponding experimental and simulation data obtained in the present case (aluminum substrate) is already shown in Fig. 6 for Re = 850 and Re = 100. The simulated heat flux ratio ϕ for these two cases is also reported on the secondary-ordinate. As can be seen, the local heat flux varies considerably along the streamwise direction and the nature of this variation is a function of the conductivity ratio k_{sf} as well as the flow Reynolds number. This indicates the nature of the isotherms, as were shown earlier in the respective insets of Fig. 6a–d. Very early part of the thermal entry length, the heat flux ratio ϕ is higher than 1; as the flow proceeds in the channel, ϕ goes below unity. The area under the $\phi - z^*$ curve, when multiplied by the area ratio of the fluid-substrate interface (A_{hp}) to the base area of the substrate (A_b), represents the constant linear heat input q'' applied at the base of the substrate. Looking at the simulated results for axial variation of local Nusselt number for the two cases ($k_{sf} = 300$ and 26.6, respectively) and comparing it with the case of thermally developing flow under uniform heat flux conditions applied on three sides, it is noted that local Nusselt number is not very sensitive to k_{sf}, except somewhat at high Reynolds number, which corresponds to very early thermal boundary layer development zone. This is due to the fact that, although the local heat flux does not remain constant at the fluid–solid interface, the temperature difference between the wall and the fluid also changes in a way that Nu_z is only mildly affected. It must be emphasized that if an experimental facility does not allow the estimation or direct measurement of local heat flux, the estimation of local Nusselt number in all such experiments, if based on gross averaged heat flux, will lead to serious errors even if the local wall temperatures have indeed been measured. To highlight this, Fig. 8 shows the corresponding wall and fluid temperatures for these two cases, respectively. The experimentally obtained wall temperature profile is also shown. As a reference case, the temperature profile for the UHF condition applied at the fluid–solid interface is also drawn. It is clearly seen that due to axial conduction in the substrate, there is a tendency of isothermalization of the wall

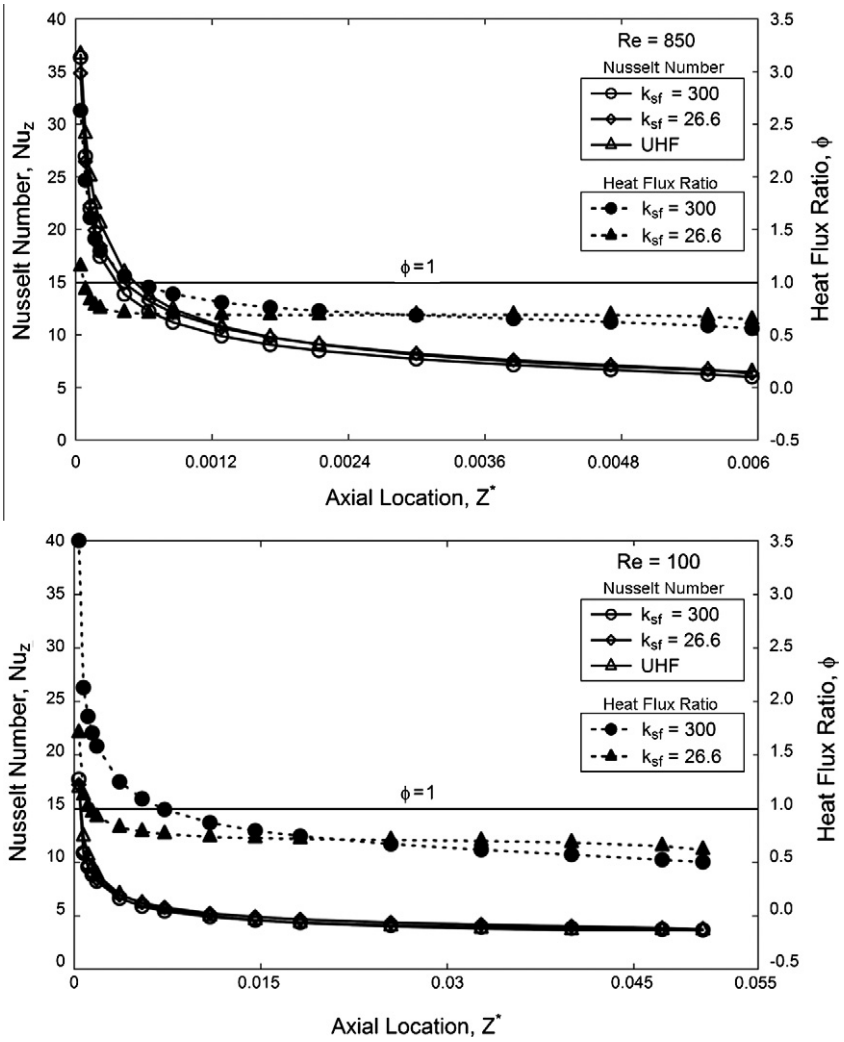

Fig. 7. Simulations of local Nu_z and heat flux ratio (ϕ), for different Re and k_{sf} ratio. k_{sf} = 300 corresponds to an aluminum substrate while k_{sf} = 26.6 corresponds to a stainless steel substrate (working fluid = water).

temperature with increasing k_{sf}. In addition, as the heat flux does not remain constant at the fluid–solid interface, as noted earlier, the increase of fluid temperature, as it passes through the channel becomes non-linear. It is rather difficult to experimentally capture this non-linearity of the fluid temperature without disturbing the velocity boundary layers. Most researchers therefore assume a linear variation of the fluid temperature.

Thus, it is noted that during experimental estimation of local Nusselt number in real-time situations, especially for developing flows, serious errors may creep in due to (i) non-availability of local heat flux due to the experimental technique applied and thus relying on some average value (ii) ignoring the effect of axial conduction and applying insufficient data points for the axial variation of wall temperature, and, (iii) assuming linear variation of the fluid temperature, which, in actual flow conditions may be non-linear. Fig. 9 shows the estimation of local Nusselt number for flow Re = 850 and 100 with three cases Case #1: True local Nu_z with local flux, exact local wall temperature and exact local fluid temperature; Case #2: All other conditions same as Case #1, but now using average value of applied constant heat flux for the entire channel; Case #3: All other conditions same as Case #1, but now using average value of applied constant heat flux for the entire channel and assuming linear variation of fluid temperature. It is clear that whenever our estimation procedure deviates from Case #1, the local Nu_z is overestimated for some region of the channel and underestimated for the rest of the channel. As is clearly observed in the Fig. 9a, Nu_z for Case #2 and Case #3 are lower than the actual Nu_z for approximately one-third length of the channel from the inlet and after that it is more than the correct value, as given by Case#1. Here, it can also be seen that, keeping all the other conditions identical but only using the linear approximation of the fluid temperature (Case #2 and Case #3), change in the numerical value of Nu_z is not significant at both higher and lower values of flow Re. Fig. 9b shows that significant errors can occur in the estimation of local Nu_z when the Re is low for Case #2 and Case #3. At lower Re, it has been observed earlier that isothermalization of the channel wall temperature is significant. Thus, the fluid temperature variation no longer remains linear. If the local Nu_z is calculated by considering constant heat flux at the solid–fluid interface, as done in Case #2 and Case #3, then the obtained estimation of Nu_z is completely wrong. This is due to the fact that moving in the streamwise direction, the temperature difference between the wall and the fluid actually decreases. Considering constant heat flux at the channel wall, the local heat transfer coefficient in the downstream location will numerically increase. This leads to a wrong estimation as the local variation of heat flux in the conjugate case gets ignored. This necessitates

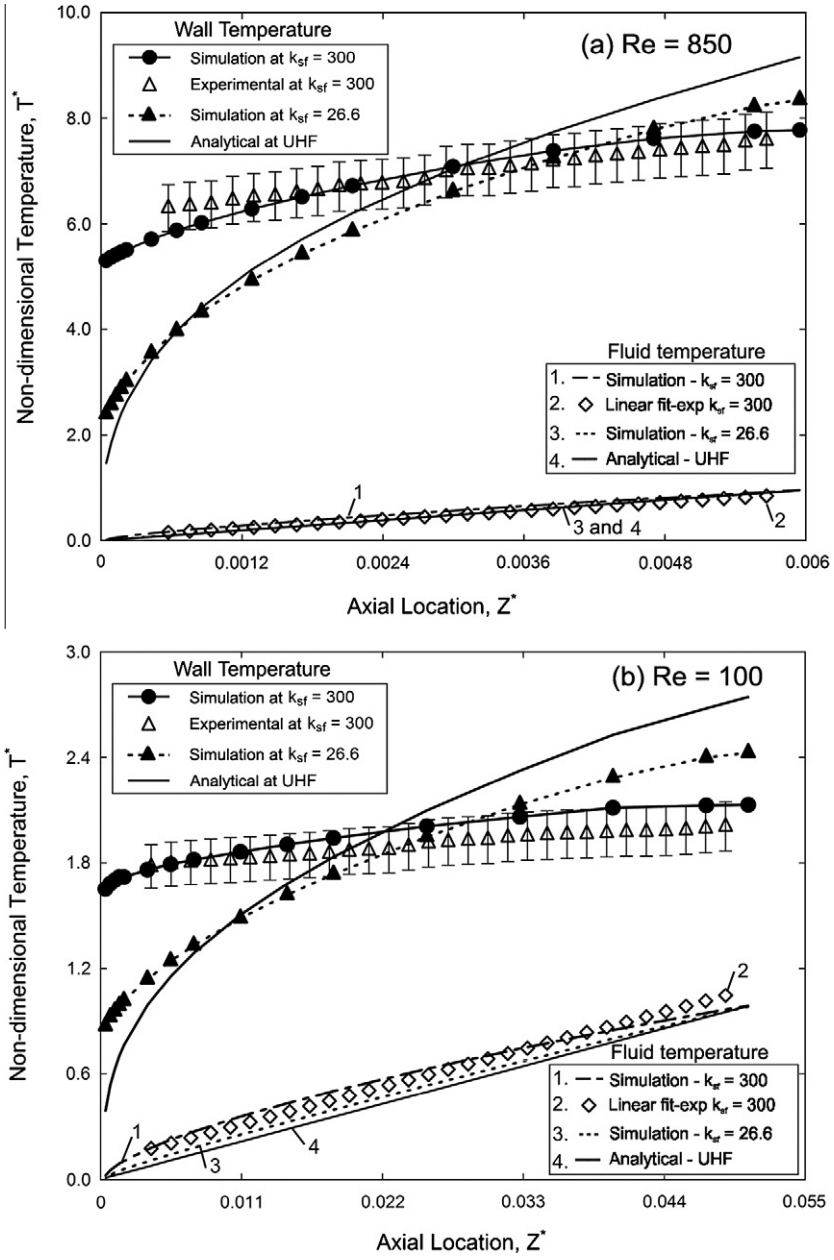

Fig. 8. Comparisons of experimental and simulated wall temperature for different k_{sf} ratio (a) Re = 850. (b) Re = 100.

correct estimation of local heat flux which can only be achieved by non-intrusive field measurement of wall temperature profile.

Microscale systems usually have a large A_{sf} and the flow Reynolds number is also low. Depending on the application, the k_{sf} value may also vary substantially; for example, biological applications may require soft and low thermal conductivity PDMS/polymer materials while microscale catalytic reactors and micro-heat exchangers may use stainless steel or copper as the substrate material. In the background of the present study, prospective designers should be aware of the detrimental effect of conjugate heat transfer which may affect microscale systems, an example of which has been recently reported by Chein et al. [28]. A thorough discussion on the interplay of A_{sf}, k_{sf}, and flow Re on conjugate heat transfer in internal convective micro-channel flows has also been recently reported by Moharana et al. [29].

7. Summary and conclusions

Thermo-hydrodynamic study of thermally developing single-phase laminar flow of water through a square mini-channel has been experimentally carried out. The main conclusions are:

(a) Developing flows provide very high heat transfer coefficients in the entrance regions and therefore of interest for mini/micro scale high heat flux removal applications.
(b) IR thermography is successfully employed to experimentally determine local Nu_z during the early thermal development region. This has been achieved as non-intrusive field measurement of local wall temperature profile is possible by IRT, which essentially provides high resolution local heat flux along the flow direction; such estimation is not achievable with intrusive conventional measurement techniques,

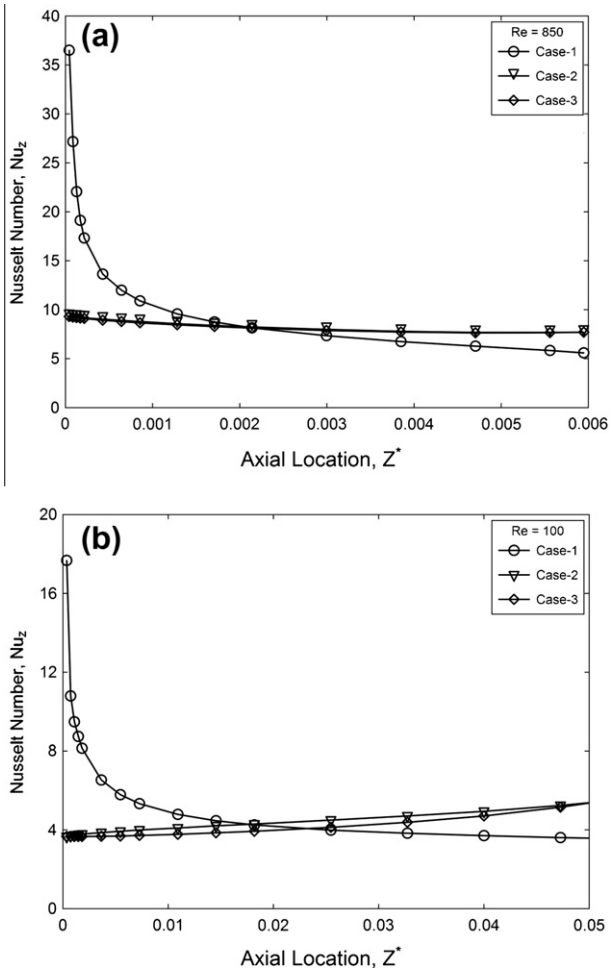

Fig. 9. Comparison of local Nusselt Number, obtained with different conditions (a) Re = 850 (b) Re = 100.

especially, when the problem is conjugate in nature. Experimental local Nu_z shows reasonable agreement with computations.

(c) Simulations reveal that if the applied heat flux is at a finite distance from the solid–fluid interface, conjugate heat transfer situations exist wherein a combination of higher k_{sf} and a lower flow Re leads to the isothermalization of interface wall temperature. In contrast, a lower k_{sf} and higher Re approaches to a constant heat flux condition at the fluid–solid interface.

(d) Nusselt numbers for UHF and the conjugate problems were numerically compared and it was shown that the deviation is not very high despite the wall and fluid temperatures deviating respectively in these two cases. Most real-time practical applications of mini–micro channel flows will lead to conjugate heat transfer scenarios. Under such conditions, it is concluded that considering a constant value of heat flux at the wall, for the entire channel length, will introduce significant errors in the estimation of local Nu_z. Therefore, correct estimation of the local heat flux is of extreme importance especially, at the lower Re and higher k_{sf}.

Acknowledgements

Financial grants from (i) Department of Science and Technology (IRHPA/FIST funding) and (ii) Indo-French Center for Promotion of Advanced Research (IFCPAR) are gratefully acknowledged.

References

[1] R.K. Shah, A.L. London, Laminar Flow Forced Convection in Ducts, Academic Press, New York, 1978.
[2] G. Maranzana, I. Perry, D. Maillet, Mini- and micro-channels: influence of axial conduction in the walls, Int. J. Heat Mass Transfer 47 (2004) 3993–4004.
[3] M. Rao, S. Khandekar, Simultaneously developing flows under conjugated conditions in a mini-channel array: liquid crystal thermography and computational simulations, Heat Transfer Eng. 30 (2009) 751–761.
[4] M.K. Moharana, G. Agarwal, S. Khandekar, Axial conduction in single-phase simultaneously developing flow in a rectangular mini-channel array, Int. J. Therm. Sci. 50 (2011) 1001–1012.
[5] S.R. Sargent, C.R. Hedlund, P.M. Ligrani, An infrared thermography imaging system for convective heat transfer measurements in complex flows, Meas. Sci. Technol. 9 (1998) 1974–1981.
[6] M. Klassen, M.D. Marzo, J. Sirkis, Infrared thermography of dropwise evaporative cooling, Exp. Fluid Therm. Sci. 5 (1992) 136–141.
[7] G. Hetsroni, R. Rozenblit, L.P. Yarin, A hot-foil infrared technique for studying the temperature field of a wall, Meas. Sci. Technol. 7 (1996) 1418–1427.
[8] T. Astarita, G. Cardone, G.M. Carlomagno, C. Meola, A survey on infrared thermography for convective heat transfer measurements, Opt. Laser Technol. 32 (2000) 593–610.
[9] G. Hetsroni, M. Gurevich, A. Mosyak, R. Rozenblit, Surface temperature measurements of a heated capillary by means of an infrared technique, Meas. Sci. Technol. 14 (2003) 807–814.
[10] S. Montelpare, R. Ricci, An experimental method for evaluating the heat transfer coefficient of liquid-cooled short pin fins using infrared thermograph, Exp. Fluid Therm. Sci. 28 (2004) 815–824.
[11] N. Kakuta, K. Kondo, A. Ozaki, Y. Arimoto, Y. Yamada, Temperature imaging of sub-millimeter-thick water using near infrared camera, Int. J. Heat Mass Transfer 52 (2009) 4221–4228.
[12] J.M. Buchlin, Convective heat transfer and infra-red thermography (IRth), J. Appl. Fluid Mech. 3 (2010) 55–62.
[13] G. Hetsroni, A. Mosyak, E. Pogrebnyak, R. Rozenblit, Infrared temperature measurements in micro-channels and micro-fluid systems, Int. J. Therm. Sci. 50 (2011) 853–868.
[14] D. Brutin, B. Sobac, F. Rigollet, C.L. Niliot, Infrared visualization of thermal motion inside a sessile drop deposited onto a heated surface, Exp. Fluid Therm. Sci. 35 (2011) 521–530.
[15] V.A. Hemadri, A. Gupta, S. Khandekar, Thermal radiators with embedded pulsating heat pipes: Infra-red thermography and simulations, Appl. Therm. Eng. 31 (2011) 1332–1346.
[16] FLIR SYSTEMS, User Manual "ThermoVision® SC4000/SC6000", 24795-000, 2007.
[17] P.S. Lee, S.V. Garimella, D. Liu, Investigation of heat transfer in rectangular microchannels, Int. J. Heat Mass Transfer 48 (2005) 1688–1704.
[18] P.S. Lee, S.V. Garimella, Thermally developing flow and heat transfer in rectangular microchannels of different aspect ratios, Int. J. Heat Mass Transfer 49 (2006) 3060–3067.
[19] G.P. Celata, M. Cumo, V. Maconi, S.J. McPhail, G. Zummo, Microtube liquid single phase heat transfer in laminar flow, Int. J. Heat Mass Transfer 49 (2006) 3538–3546.
[20] Z. Liu, Y. Zhao, M. Takei, Experimental study on axial wall heat conduction for convective heat transfer in stainless steel microtube, Heat Mass Transfer 43 (2007) 587–594.
[21] C. Nonino, S. Savino, S. Giudice-Del, L. Mansutti, Conjugate forced convection and the heat conduction in circular microchannels, Int. J. Heat Fluid Flow 30 (2009) 823–830.
[22] C. Fan, Unsteady, laminar, incompressible flow through rectangular duct, ZAMP 16 (1965) 351–360.
[23] K.D. Cole, C. Tarawneh, B. Wilson, Analysis of flux-base fins for estimation of heat transfer coefficient, Int. J. Heat Mass Transfer 52 (2009) 92–99.
[24] O. Aydin, L. Guessous, Fundamental correlation for laminar and turbulent free convection from uniformly heated vertical plate, Int. J. Heat Mass Transfer 44 (2001) 4605–4611.
[25] T. Audunsun, B. Gebhart, An experimental and analytical study of natural convection with appreciable radiation effects, J. Fluid Mech. 52 (1972) 52–95.
[26] M. Renksizbulut, H. Niazmand, Laminar flow and heat transfer in the entrabce region of trapezoidal channels with constant wall temperature, ASME J. Heat Transfer 128 (2006) 63–74.
[27] Y.S. Muzychka, M.M. Yovanovich, Pressure drop in laminar developing flow in noncircular ducts: a scaling and modeling approach, ASME J. Fluid Eng. 131 (2009) 111105-1–111105-11.
[28] R. Chein, Y. Chen, J.N. Chung, Axial heat conduction and heat supply effects on methanol-steam reforming performance in micro-scale reformers, Int. J. Heat Mass Transfer 55 (2012) 3029–3042.
[29] M.K. Moharana, P.K. Singh, S. Khandekar, Optimum Nusselt number for simultaneously developing internal flow under conjugate conditions in a square microchannel, ASME J. Heat Transfer 134 (2012) 071703-1–071703-10.